The current issue and full text archive of this journal is available at
www.emeraldinsight.com/0961-5539.htm

Parallel computation of multiscale phenomena in magnetically-stirred solidifying melts

Ben Q. Li
School of Mechanical and Materials Engineering, Washington State University, Pullman, Washington, USA

Received 5 December 2005
Revised 2 January 2007
Accepted 2 January 2007

Abstract

Purpose – The aim of this paper is to determine a parallel computational methodology for simultaneously predicting the macro/micro scale phenomena occurring during solidification processing with external electromagnetic stirring.

Design/methodology/approach – Macro and micro phenomena occurring in an electromagnetically-stirred solidifying melt are simulated using a numerical model that integrates the finite element methodology for transport phenomena and the Monte-Carlo cellular-automata method for microstructure formation. Parallel algorithm is introduced to enhance the computational efficiency.

Findings – Computed results show that parallel algorithm can be effective in enhancing the computational efficiency of a combined macro/micro model if it is applied appropriately. Also, electromagnetically induced stirring can have a strong effect on the nucleation and grain growth and hence the final solidification microstructure.

Originality/value – This paper fulfils a need for developing an efficient numerical methodology to simulate complex electromagnetically-assisted transport phenomena and microstructure formation during solidification processing systems.

Keywords Numerical analysis, Modelling, Electromagnetism, Flow

Paper type Research paper

Nomenclature

$\mathbf{B}$ = magnetic field
$\mathbf{D}$ = electric displacement
D_1 = diffusion coefficient
$\mathbf{E}$ = electric field
F_{sl} = damping force from solidification
f = solid fraction
H = latent heat of solidification
$\mathbf{J}$ = current density
K = partition coefficient
k = thermal conductivity
m = slope of solidus-liquidus line
n = number of sites nucleated per unit volume
n_{max} = nucleation site density
p = pressure
Q_{em} = Joule heating
T = temperature
ΔT = undercooling
ΔT_σ = mean undercooling
t = time
$\mathbf{u}$ = velocity vector

The author gratefully acknowledges the support of this work by the US National Aeronautics and Space Administration (Grant No: NAG8-NNM04AA17G).

International Journal of Numerical Methods for Heat & Fluid Flow
Vol. 18 No. 2, 2008
pp. 131-145

0961-5539
DOI 10.1108/09615530810846293

Greek letters
Γ = Gibbs-Thomson coefficient
μ = magnetic permeability
μ_{eff} = effective viscosity
ρ = density
σ = electrical conductivity

Subscripts
eff = effective

Introduction

It is well known that strong flow induced by electromagnetic stirring can be used to control solidification microstructures and to reduce or eliminate solidification defects such as subsurface inclusions, pinholes, blowholes, internal cracks, center-line segregation, porosity and V-segregation (Vives, 1990; Marr, 1979). During solidification, the liquid-to-solid transformation starts with nucleation that comes from the clustering of molecules, followed by deposition of molecules upon the nuclei or grain growth. In materials dynamics, these events are modeled at a spatial scale of microns and a temporal scale of micro seconds. On the other hand, the electrodynamic, fluid flow and heat transfer phenomena in solidifying metals are observable and thus modeled at a scale of millimeters (or sometimes centimeters) and a fraction of a second. It is well known that the fluid flow and temperature distributions have significant effects on the formation of microstructure in solidifying melts in two major ways. First, the strong flow distorts the temperature distribution and quickly distributes the latent heat released from the solidification front to the bulk melt. Second, a strong stirring can result in remelting of an already solidified metal, and if strong enough, can break the newly formed dendrites, which can serve as nucleation sites when carried into the melt by convection. The transformation of the liquid to solid, on the other hand, changes the local resistance to the flow field. Magnetically driven flows and microstructure formation have been studied as separate subjects in extensive literature. However, there has not yet been an integrated computational methodology to quantify the effects of strong magnetically induced macro flows on solidification microstructures. Although they occur at the temporal and spatial scales of a great disparity, these macro- and micro-scale phenomena are intimately related. This has been demonstrated by some of the recent work on macro/micro modeling of solidification processes without external stirring (Cabrera-Marrero *et al.*, 1998; Stefanescu, 2002; Kraft, 1997).

This paper presents an integrated macro/micro model for magnetically-driven flow and heat transfer along with the formation of solidification microstructures, in order to quantify the effect of flow behavior on microstructure formation in electromagnetically stirred solidifying melts. The model is developed based on the parallel computing platform. The model should be useful to further our fundamental understanding of flow and microstructure formation in electromagnetically-assisted processes such as electromagnetic casting, arc welding, and vacuum refining.

Problem formulation

Consider a simple (2D), idealized, unidirectional solidification system, three sides of which are insulated and cooling is applied on the fourth side (Figure 1). Initially, the metal alloy (Al-4.5%Cu) is above its melting point and solidifies as the heat is drawn from the right side. The solidifying alloy is stirred by induced electromagnetic forces, which are produced by the coils arranged as shown in Figure 1. AC currents are applied in the z-direction, which is perpendicular to the plane of the paper.

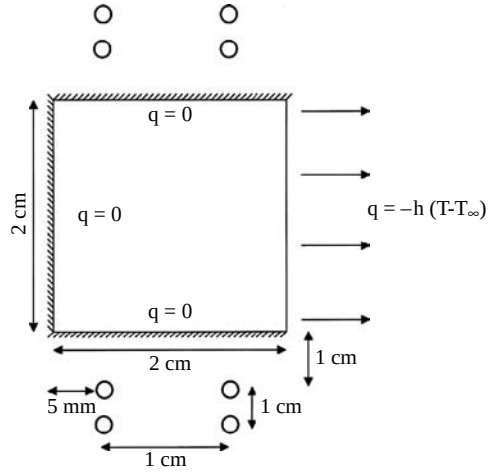

Figure 1.
Schematic representation of solidification with induction stirring

Because the electromagnetic forces are vortical in nature, recirculating flows will be generated (Li, 1994). The mathematical formulations governing these phenomena consist of the Maxwell equations for electrodynamics, the Navier-Stokes equations for fluid flow, the thermal balance equation for heat transfer, and nucleation and grain growth calculations. Because of a lack of detailed kinetics models for the dendrite shearing by fluid flow, the convective transport of the debris is not considered in the present study. Of course, this feature can be readily incorporated when the detailed information on flow interaction with dendrites are known. The macro-scale equations may be written as follows, with symbols carrying the definitions used in standard textbooks (Jackson, 1968; Batchelor, 1966):

$$\nabla \times \mathbf{E} = -\frac{\partial \mathbf{B}}{\partial t} \tag{1}$$

$$\nabla \times \mathbf{B} = \mu \mathbf{J} + \frac{\partial \mathbf{D}}{\partial t} \tag{2}$$

$$\nabla \cdot \mathbf{B} = 0 \tag{3}$$

$$\nabla \cdot \mathbf{J} = 0 \tag{4}$$

$$\mathbf{J} = \sigma(\mathbf{E} + \mathbf{u} \times \mathbf{B}) \tag{5}$$

$$\rho \frac{\partial \mathbf{u}}{\partial t} + \rho \mathbf{u} \cdot \nabla \mathbf{u} = -\nabla p + \nabla \cdot (\mu_{\text{eff}} \nabla \mathbf{u}) - \rho \beta g (T - T_r) + \mathbf{J} \times \mathbf{B} + F_{\text{sl}} \tag{6}$$

$$\nabla \cdot \mathbf{u} = 0 \tag{7}$$

$$\rho C_p \frac{\partial T}{\partial t} + \rho C_p \mathbf{u} \cdot \nabla T = \nabla \cdot (k_{\text{eff}} \nabla T) + \rho H \frac{\partial f}{\partial t} + Q_{\text{em}} \tag{8}$$

For the F_{sl} term, the Carman-Kozney equation is used (Voller and Brent, 1989), where the effect of detailed mushy zone microstructure is lumped into the solid fraction. Also, the above equations, μ_{eff} and k_{eff} depend on the fluid flow conditions.

The above equations are subject to appropriate boundary conditions. The boundary conditions for the electromagnetic fields are such that both tangential and normal components of the magnetic and electric fields are continuous at the interface between the air and metal, and they diminish to zero infinitely far away from the coil-metal assembly. At the walls, the no-slip conditions are applied for the velocity. The thermal boundary conditions are as shown in Figure 1.

For the binary alloy under consideration, the microscopic events, i.e. the nucleation and subsequent grain growth, may be described by the following set of mathematical equations (Govindaraju, 2000; Song, 1999; Rappaz and Gandin, 1993):

$$\frac{\mathrm{d}n}{\mathrm{d}(\Delta T)} = \frac{n_{\max}}{\Delta T_\sigma \sqrt{2\pi}} \exp\left[-\left(\frac{[\Delta T - \Delta T_{\max}]}{\sqrt{2}\Delta T_\sigma} \right)^2 \right] \tag{9}$$

$$\lambda_i = 2\pi \sqrt{\frac{\Gamma}{\phi}} \tag{10}$$

$$\Omega = Pe_t \tag{11}$$

$$Pe_t = \frac{v_s R_t}{2D_l} \tag{12}$$

$$R_t = \lambda \tag{13}$$

$$\Delta T = mc_0 \left[1 - \frac{1}{1 - \Omega(1 - K)} \right] \tag{14}$$

Note that equation (9) is an empirical expression for nucleation where $n_{\max}$ and ΔT_σ are obtained from fitting with the data of solidification microstructure measurements (Song, 1999; Rappaz and Gandin, 1993).

Numerical solution

The above equations are solved by computational software developed by our research group over the past ten years. The electromagnetic field equations are solved using a hybrid boundary element and finite element (BE/FE) method. The fluid flow and heat transfer equations are solved using the FE method employing the backward Euler (or implicit) time difference scheme with automatic time-step control and the penalty method for pressure approximation (Gandin and Rappaz, 1994). The nucleation and grain growth phenomena are simulated using the cellular automaton (CA) method (Song, 1999; Rappaz and Gandin, 1993). The coupling of the macro and micro calculations is made through the sub-level time and space division scheme (Govindaraju, 2000; Rappaz and Gandin, 1993; Li and Anyalebechi, 1995; Rappaz, 1989). As details of the solution methods are well documented elsewhere, only an outline is given here.

The Maxwell equations are reformulated in terms of vector potential for the present problem, within the MHD framework (Song and Li, 2000). For the problem under consideration, the vector potential has only z-component $\mathbf{A} = (0,0, \mathbf{A}_z)$, where $\mathbf{B} = \nabla \times \mathbf{A}$, and its governing equation simplifies to a Poisson equation for the outside of the metal and a Helmholtz equation for the inside. The space outside the metal

is modeled by the BE method that takes the boundary condition at infinity into formulation directly and thus eliminates the need to discretize the outside domain extending to infinity. This results in considerable savings in computing time, memory requirement and storage space. Inside the metal the vector potential is solved using the FE method. This allows us to obtain directly from the numerical solution the detailed distributions of the Lorentz force and Joule heating sources required to compute the fluid flow and temperature distribution (Shu *et al.*, 2005). It is noted that the elements of the global matrix for the vector potential resulting from the hybrid boundary and FE formulation as described above are complex numbers because of the use of the phasor notation to describe the vector potential. This matrix is sparse and stored in the skyline format. Its bandwidth is determined by the nodal points along the boundary. Thus, the optimal node arrangement in the system is important for numerical computation. Experience shows that optimal efficiency is achieved if the FEs are arranged in such a way that the nodes are numbered spirally inward starting from the interface nodes between the BE and FE regions. The solution of the matrix can be obtained using the complex LU decomposition method.

The fluid flow and heat transfer equations are solved using the Galerkin FE method with the Lorentz force and Joule heating treated as sources for momentum and energy balance. The FE code used for thermal and fluid flow computations was also developed by our group. The code for fluid flow and thermal phenomena was tested for accuracy against other available commercial codes and the analytical solutions for a wide variety of flow and thermal problems and also against experimental measurements (Song and Li, 2000; Shu *et al.*, 2005). The code has a variety of elements in its element library and various choices for pressure approximation. In the present study, the four-node element is chosen and the pressure is approximated by the penalty formulation. The four-node element in general is considered more useful for solidification calculations that involve complicated and highly non-linear terms resulting from the latent heat release and liquid-to-solid transformation.

The Monte-Carlo cellular-automaton method is used for computation of solidification microstructure evolution, which is described by equations (9)-(14). The basic algorithm used in this study follows that proposed by Gandin and Rappaz (Song, 1999; Rappaz and Gandin, 1993) and is documented in detail elsewhere (Govindaraju, 2000). It involves treating nucleation by the Monte-Carlo method and grain growth by the CA method. Nucleation on the walls and in the bulk is modeled using a Gaussian distribution, the location of the nucleated sites and their orientation being randomly chosen (taking into account the four-fold symmetry of the dendrite) (Song, 1999; Rappaz and Gandin, 1993). The growth kinetics is computed following the algorithm developed by Rappaz and Gandin (1993). In order to simulate the microstructure evolution, the domain of concern is split into a number of CA cells small enough to represent the branching mechanisms of the dendrites (Figure 2), along with a smaller time-step (compared to the macro-scale calculations). Direct use of these small time-steps and space discretization for computation of the macroscopic equations would make the model prohibitively expensive. To circumvent this difficulty, a sub-level time and space scheme for macro/micro coupling is used (Li and Anyalebechi, 1995) wherein a macro time-step is employed for heat and fluid flow calculations and a micro time-step for microstructure calculations. For each micro time-step, the undercooling for each CA cell is calculated by interpolating the temperature at the nodes of the element to the center of the CA cell. The solid fraction, for each element,

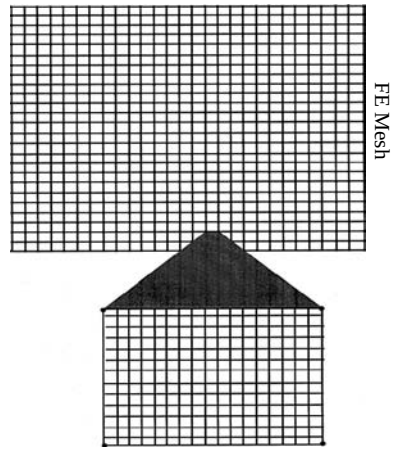

Figure 2.
Meshes of FE and cellular-automata for solidification modelling

calculated using the CA model, at the end of each macro time-step is used to calculate the latent heat release and the phase interaction effects on fluid flow using Carman-Kozney equation. It should be noted that the micro time-step should be small enough so that the dendrite tip extension never exceeds the cell spacing.

Experience with numerical simulations shows that the macro/micro calculations as described above are extremely (and very often prohibitively) computationally intensive and that the CA simulations are the most expensive part, largely because of the very fine spatial discretizations. To circumvent this difficulty, a parallel algorithm was designed and implemented. For the present study, the parallel algorithm was implemented using the parallel virtual machine (PVM) library and calculations were done on an SGI machine with six processors. The parallel algorithm for macro/micro calculations is presented below.

Parallel computing

We devote our attention here to parallelize the micro scale computations only for the two reasons. First, for the problem under consideration, the FE computations take a negligible fraction of the total time and also the basic ideas for parallel FE computing have been discussed in literature. Second, our numerical experience shows that the simulation of solidification microstructure constitutes the speed bottleneck for the coupled macro/micro computations.

Two widely practiced parallel computing algorithms are crowd and tree computations. Crowd computations are further classified into master-slave (or master-worker) and node only algorithms. The master-slave approach involves two sets of processes: a master task and multiple slave tasks. The master process is in charge of the overall computation while the actual computation is done by slave tasks. The master task first sets up the problem, creates the slave tasks, distributes work load to the tasks and collects the results. The master task may itself perform a part of the computation if there is considerable delay between work allocation and collection of results. Each slave task for its part receives the data it requires for computation from the master, performs the calculations and

returns the result to the master. The slave tasks, depending on the problem being solved, may or may not need to communicate among themselves. Any such communication is an overhead to computation. It should be noted in the case of master-slave computing the master and slave programs can be completely different. In the case of node only computations multiple copies of the same program execute, with one process doing the non-computational work (in addition to doing computation) while the rest of the processes do the computation.

For tree computations, the process flow-structure resembles that of tree – a single process starts multiple tasks, and allocates some work to them, while it does computations. The "second generation" of tasks in turn starts more tasks allocating some portion of their work. This process is continued until the problem is solved.

For the coupled macro/micro computations of magnetically-driven flows and microstructure formation under consideration, the master-slave parallel algorithm is most suitable. This is because the master-slave structure is apparently inherent in these computations. The FE code for simulating the macroscopic phenomena can be treated as the master while microscale calculations are performed by the slave tasks. The functions performed by each task, i.e. a single master and a set of slaves, are discussed below.

Master task

For every macro time-step the master task estimates the number of elements for which microstructure computations need to be performed. This is done by looping through all the elements in the mesh and considering only those elements which are within the limits $T_e < T < T_l$, where T_e is the eutectic temperature and T_l the liquidus temperature of the alloy, respectively.

Let NPROC be the number of elements (i.e. slave tasks) which fall within the above range and NPRS be the number of processors available for computation. Directly starting NPROC tasks (actually the total number of processes will be NPROC + 1 including the master) on NPRS processors will be efficient only if (NPROC + 1) $\leq$ NPRS. For the solidification problems, it is not possible to decide NPROC a priori, since it depends on the temperature distribution in the melt which in turn can vary in any number of ways depending on the applied boundary conditions and the distribution of electromagnetic forces among others. This problem is alleviated by allowing defining the maximum number of slave processes, NFIX, which is spawned by the master. This ensures maximum possible flexibility: the algorithm can be used on either a single processor machine or multiprocessor machine; either using all the resources or only a portion of the resources.

For each macro time-step the master estimates NPROC, but spawns only NFIX iteratively until all of the NPROC elements are covered. Asynchronous communication is used when sending data needed for computation to slaves, while synchronous communication is used when receiving computed data from the slaves. This ensures that minimum amount of time is spent while sending data to slaves, but at the same time taking care the computation does not proceed to subsequent macro time-steps without receiving microstructure data for the current (macro) time-step. For the problem considered here, the master task also performs all input/output operations, FE calculations and task management.

Slave tasks

As stated earlier, the most intensive computations for this type of problems come from the Monte-Carlo cellular-automation simulation of solidification microstructure formation over each element undergoing phase change. Figure 3 shows a schematic representation of grain growth extending across the boundaries of an element. To ensure the continuity of grain growth across element boundaries, it is necessary for the slave tasks to communicate with each other. Fortunately, all of the NFIX slaves spawned need not communicate with each other. A slave task needs to communicate with a maximum of four other tasks – its nearest neighbors, as can be seen in Figure 3. The number will be less for elements adjacent to the wall.

In the macro/micro model, microscale calculations employ microscale time-steps. This implies that microstructure computations are communication-intensive in spite of the fact that a slave needs to communicate with a maximum of only four tasks. To speed up computing, all communications between slaves are made asynchronous. However, this presents a problem: the extent of growth in each of "nearest neighbor task" will not be exactly the same, resulting in some tasks completing computations faster than the rest. Consequently, the other tasks may communicate with a task no longer existing, thereby resulting in a significant loss of computing time. To alleviate this problem, provision is made to notify the nearest neighbors if a particular task has finished computations.

Spawning of NFIX processes when NFIX $<$ NPROC may result in a certain task being unable to communicate with one or more of its nearest neighbors, even though the tasks which have not yet been spawned are within the temperature range for microstructure calculations. For these cases, the spawned task at the end of its computation informs the master about the "missing" neighbors, the master in turn updates microstructure data for the neighbors if deemed necessary. The updating of the data being carried about as if the growth proceeds from the task which was spawned to the tasks which have not been spawned.

The parallel algorithm entailing the use of the master and slave tasks is shown in Figure 4, while the detailed computations and slave-slave communication are shown in Figure 5. It is noted that SFRCT in the Figure 5 refers to the solid fraction.

Results and discussion

The computational model, as described above, allows us to predict simultaneously the evolution of the electrodynamic, fluid flow and heat transfer phenomena as well as

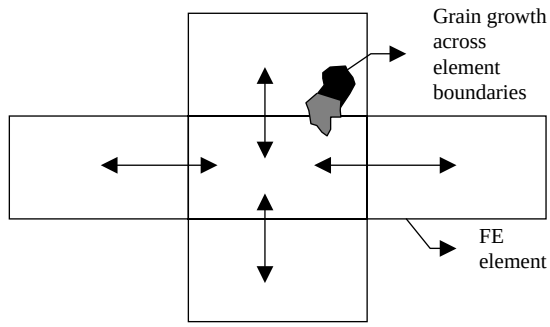

Figure 3.
Communication between slaves

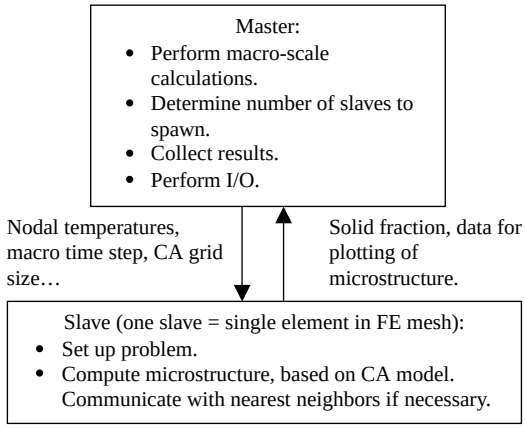

Figure 4.
Functions performed by master and slave tasks

the microstructure formation in solidifying metals. Extensive numerical simulations were conducted using the model and selected results are presented below. Before proceeding to carry out full scale simulations, it is important to validate the developed code for some simplified cases. While there are abundant examples published to check for electromagnetic, thermal and fluid flow calculations, very few computational examples are available for computation of microstructure formation. To check the Monte-Carlo cellular-automaton calculations, we have compared our simulated results with those published (Song, 1999; Rappaz and Gandin, 1993) for the simplest possible case where the metal is initially at a temperature above the melting point and is cooled uniformly throughout. As such, the detailed temperature distribution is not needed and fluid flow is not considered.

In addition, no electromagnetic stirring is applied. The computational domain was a square of 5×5 mm filled with the Al-7%Si alloy melt. The discretization consists of 300×300 cellular-automata cells, which gives a resolution of about 16 μm. The calculated result is shown in Figure 6, which is in good agreement with that reported in Rappaz and Gandin (1993), thereby providing a validation of the Monte-Carlo cellular-automaton computational methodology for microstructure formation simulations.

For the results presented below, the computations used 1,600 four-node elements (see Figure 2, only upper part of the domain shown below) and each element was divided into a 50×50 CA grid to give a grid resolution of about 10 μm (Govindaraju, 2000). The parameters used for all computations presented in this paper are given in a recent thesis (Govindaraju, 2000) and also in open literature (Stoehr and Loyprasert, 1999). The geometric dimensions for the computational domains are shown in Figure 1. It is noted here that the vector potential, fluid flow and temperature fields possess a perfect symmetry with respect to the middle plane, but such symmetry in solidification microstructure is only approximate, although the solidification front itself exhibits perfect symmetry. This is because the detailed grain structure is dependent upon the grain orientation at the micro-scale level that is determined by the local conditions near the wall as explained in Song (1999) and Rappaz and Gandin (1993).

Figure 7 shows a set of snapshots of the dynamic development of the microstructure and temperature distribution in the computational domain, without electromagnetic stirring. For this case, as it is expected, solidification starts at the right-hand wall,

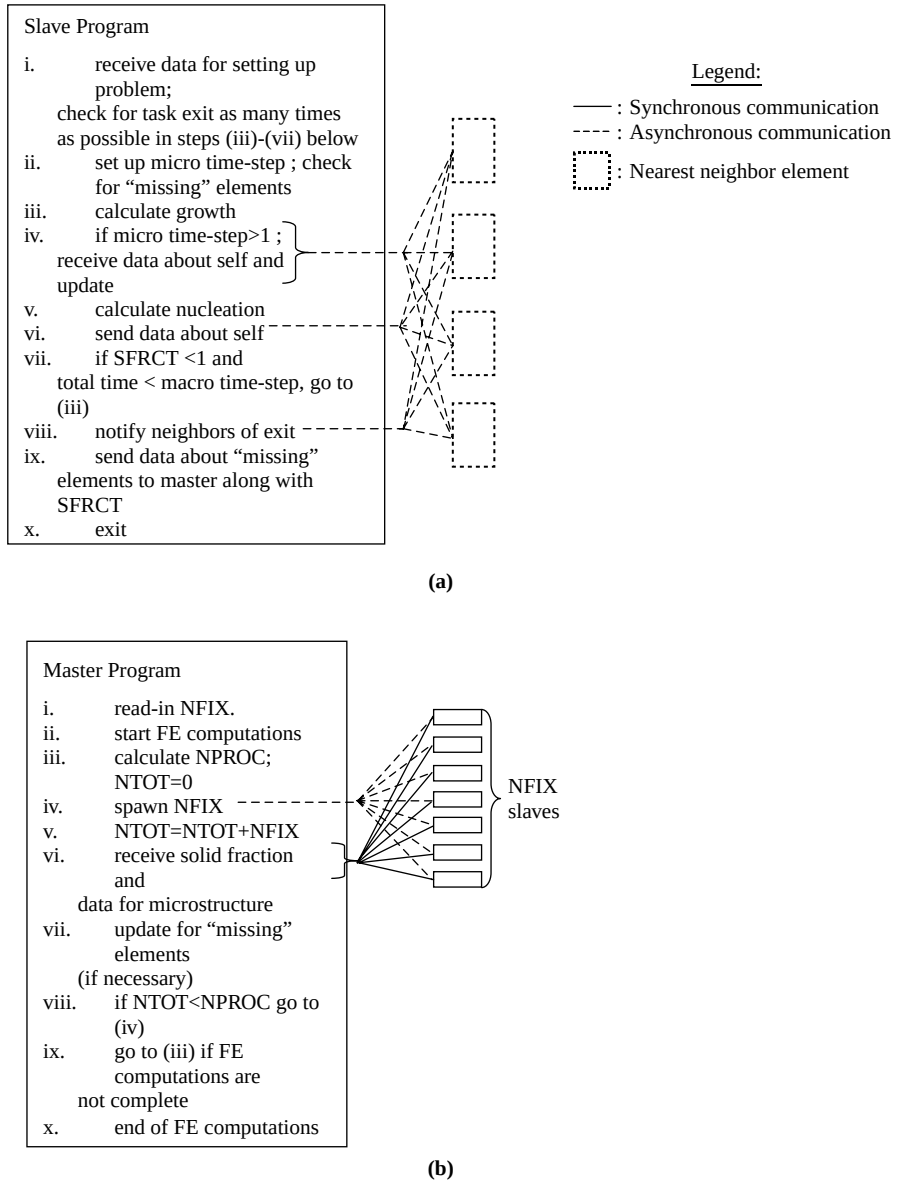

Figure 5.
Tasks performed and communication schemes used in the parallel algorithm

which is cooled by the Newton's cooling law. Nucleation first occurs along the cooling wall and grains gradually grow into the liquid as temperature drops and solidification proceeds. Since, no external stirring is applied and buoyancy is neglected, solidification progresses in the direction perpendicular to the thermal gradient. Note that the solidification front is parallel to the cooling wall, but the individual grains are not. In fact, the grain growth directions are dependent upon the local microscopic nucleation

and grain growth kinetics, along with the preferred crystallographic orientation depending on the local conditions.

The time evolution of fluid flow, temperature distribution and microstructure formation in the same system, now with electromagnetic stirring provided by external coils is shown in Figure 8. The coil arrangement is shown in Figure 1. Inspection of these snapshots illustrates that the application of the stirring has a profound effect on the solidification

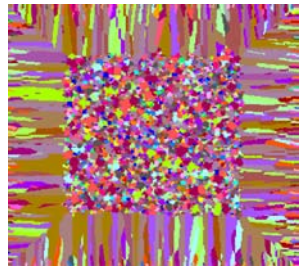

Note: The sample is uniformly cooled and no electromagnetic stirring is applied

Figure 6.
Final solidification microstructure in the final product of Al-7%Si alloy obtained using the Monte-Carlo cellular-automaton method

(a) Microstructure at time = 0.65 s

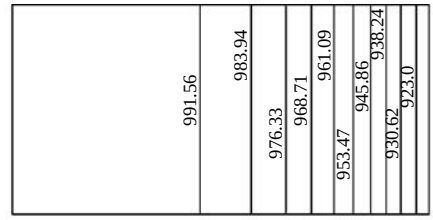

(b) Temperature contour plot at t = 0.65 s

(c) Microstructure at time = 0.95 s

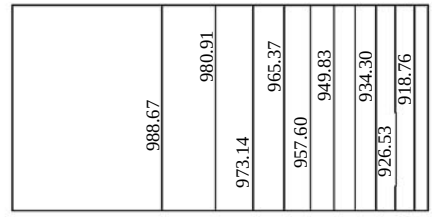

(d) Temperature contour plot at t = 0.95 s

(e) Microstructure at time = 1.75 s

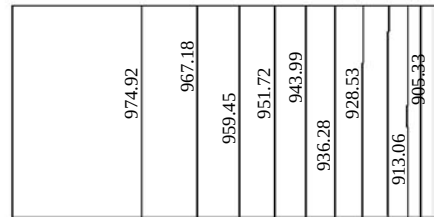

(f) Temperature contour plot at t = 1.75 s

Figure 7.
Evolution of temperature distributions and microstructure formation during solidification of Al-4.5%Si without electromagnetic stirring: $h = -3{,}000\ \mathrm{W/m^2K}$ and $T_{\mathrm{init}} = 1{,}000\ \mathrm{K}$

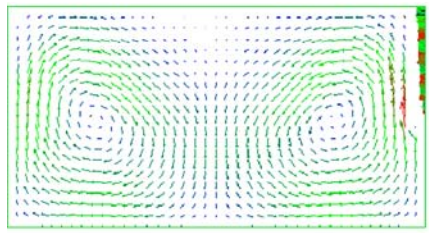

(a) Velocity plot with microstructure: t = 0.65 s; Max velocity = 0.021 m/s; Re = 342.72

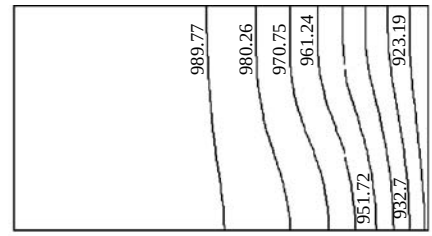

(b) Temperature contour plot at t = 0.65 s

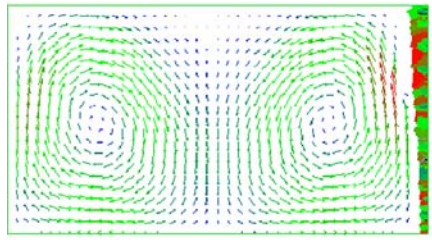

(c) Velocity plot with microstructure: t = 0.95 s; Max velocity = 0.023 m/s; Re = 375.36

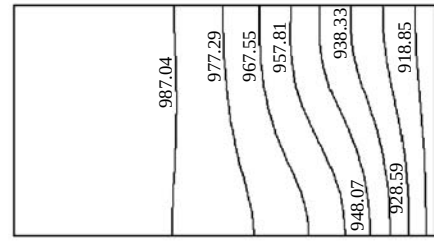

(d) Temperature contour plot at t = 0.95 s

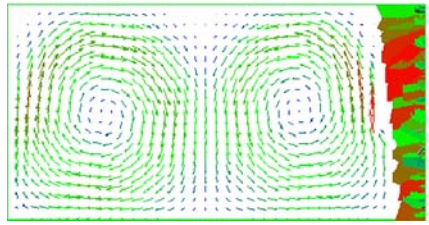

(e) Velocity plot with microstructure: t=1.75 s; Max velocity = 0.03m/s; Re = 489.6

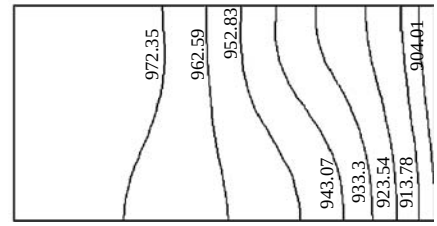

(f) Temperature contour plot at t = 1.75 s

Figure 8.
Dynamic development of magnetically driven flows, temperature distributions and microstructure formation in solidifying metals with electromagnetic stirring: $I = 200$ A; $f = 50$ Hz; $h = -3{,}000$ W/m^{2}K; $T_{\text{init}} = 1{,}000$ K

behavior of the metal, both in terms of the macroscale solidification front and microscale grain structure. The vigorous stirring results in a flow structure exhibiting two loops rotating in opposite directions and recirculating in the entire pool. The temperature field is distorted by the convective transport in the pool (as evident in the temperature contour plots) and the hot liquid is quickly moved around by the recirculating convection generated by the Lorentz forces in the melt, leading to the formation of a different solidification microstructure. Because of the flow, the solidification of the metal first appears at the upper right corner where the stirring is not fully penetrated (dead-zone area). Also, strong mixing quickly transports the hot fluid to the middle region near the symmetry line to keep temperature higher than the dead zone areas, thereby preventing solidification from taking place. Comparison with the figures without stirring indicates that some of the grains in the dead-zone grow along the solid wall in the early stage of solidification until the nucleation and growth of new grains stop them from growing continuously. As a consequence of this gain impingement, the solidification microstructure is different.

The numerical model may also be applied to study the effect of process parameters on the flow and microstructure formation. Figure 9 shows the flow and thermal fields and the microstructure that are evolving as solidification taking place. Comparison of Figures 8 and 9 show that with an increase in applied current, the flow is intensified in its recirculation. This in turn better homogenizes the melt and thus delays the solidification.

The effect of the initial melt temperature on solidification microstructure formation and fluid flow and temperature distribution in the solidifying system is shown in Figure 10. It is seen from Figure 10 that a decrease of the initial temperature helps the solidification start more quickly, as it is expected. The stronger flow in the pool, however, transports the hot fluid into the cold region more quickly. The intensified flow also helps to smooth out the solidification front. The microstructure consists mainly of slender columnar grains grow from the solid surface.

Concluding remarks

This paper has presented an integrated macro/micro model for simultaneously predicting the electromagnetic field and forces, melt flow, heat transfer and microstructure evolution in

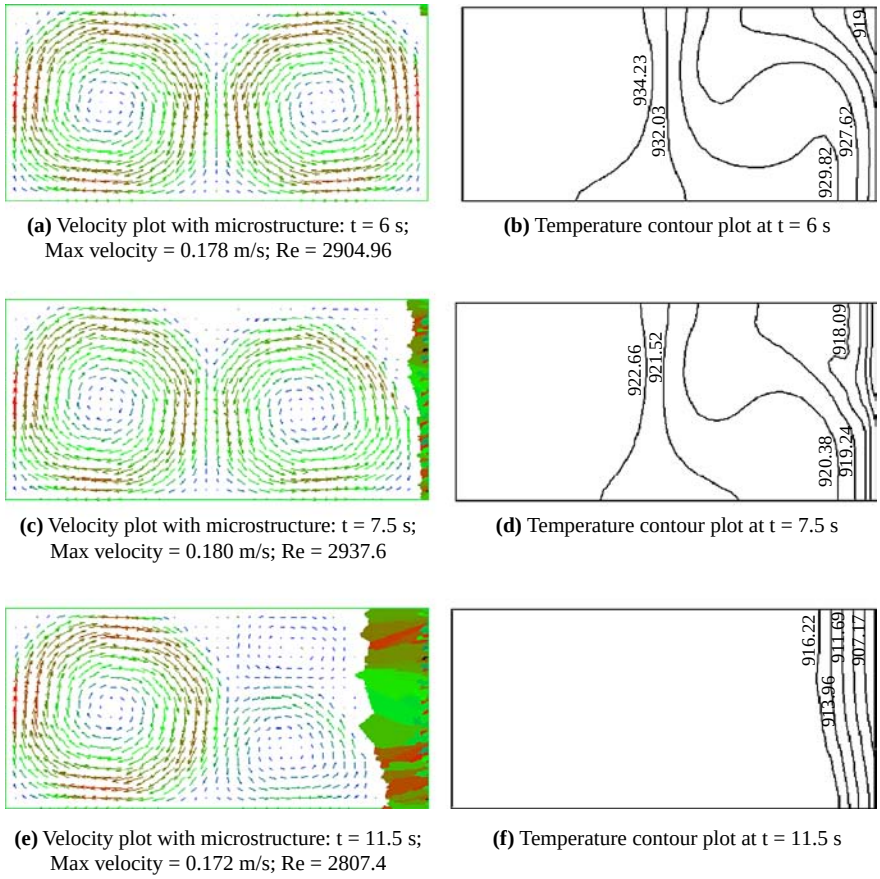

(a) Velocity plot with microstructure: t = 6 s; Max velocity = 0.178 m/s; Re = 2904.96

(b) Temperature contour plot at t = 6 s

(c) Velocity plot with microstructure: t = 7.5 s; Max velocity = 0.180 m/s; Re = 2937.6

(d) Temperature contour plot at t = 7.5 s

(e) Velocity plot with microstructure: t = 11.5 s; Max velocity = 0.172 m/s; Re = 2807.4

(f) Temperature contour plot at t = 11.5 s

Figure 9.
Evolution of magnetically driven flows, temperature distributions and microstructure formation in solidifying metals with electromagnetic stirring: $I = 800$ A; $f = 50$ Hz; $h = -3{,}000$ W/m^{2}K; $T_{\text{init}} = 1{,}000$ K

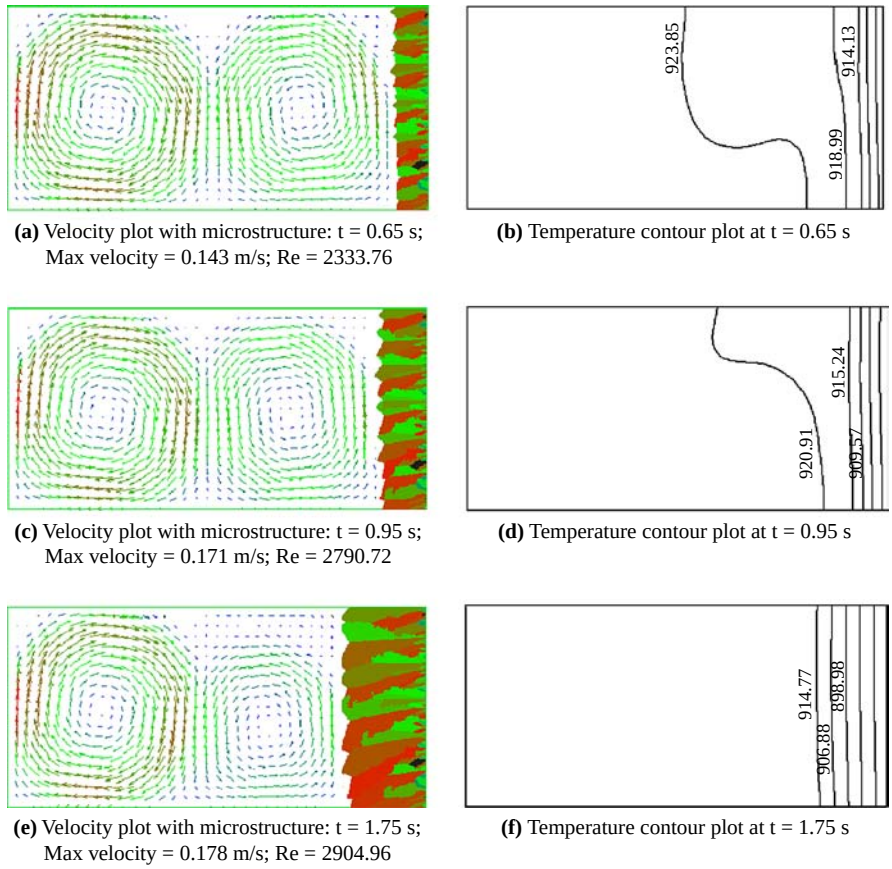

(a) Velocity plot with microstructure: t = 0.65 s; Max velocity = 0.143 m/s; Re = 2333.76

(b) Temperature contour plot at t = 0.65 s

(c) Velocity plot with microstructure: t = 0.95 s; Max velocity = 0.171 m/s; Re = 2790.72

(d) Temperature contour plot at t = 0.95 s

(e) Velocity plot with microstructure: t = 1.75 s; Max velocity = 0.178 m/s; Re = 2904.96

(f) Temperature contour plot at t = 1.75 s

Figure 10.
Evolution of magnetically driven flows, temperature distributions and microstructure formation in solidifying metals with electromagnetic stirring: $I = 800$ A; $f = 50$ Hz; $h = -3{,}000$ W/m^{2}K; $T_{\text{init}} = 930$ K

metals with electromagnetic stirring. The computational methodology is based on the hybrid BE/FE solution of the Maxwell equations and of the Navier-Stokes and thermal balance equations, along with the CA method for microstructure predictions. Parallel algorithm was also implemented using the PVM library to expedite the otherwise expensive computations. Numerical simulations were carried out using the integrated macro/micro model. Computed results show that electromagnetically induced stirring can have a strong effect on the nucleation and grain growth and hence the final solidification microstructure.

References

Batchelor, G.K. (1966), *Introduction to Fluid Dynamics*, Cambridge University Press, London.

Cabrera-Marrero, J.M., Carreno-Galindo, V., Morales, R.D. and Chavez-Alcala, F. (1998), "Macro-micro modeling of the dendritic microstructure of steel billets processed by continuous casting", *ISIJ International*, Vol. 38 No. 8, pp. 812-21.

Gandin, Ch-A. and Rappaz, M. (1994), "A coupled finite element-cellular automaton model for the prediction of dendritic grain structures in solidification processes", *Acta metallurgica et materialia*, Vol. 42, pp. 2233-46.

Govindaraju, N. (2000), "Numerical simulation of microstructure formation during solidification with magnetically driven flows using parallel computing", MS thesis, Washington State University, Pullman, WA.

Jackson, J.D. (1968), *Classical Electrodynamics*, Wiley, New York, NY.

Kraft, T. (1997), "An efficient method for coupling microscopic and macroscopic calculations in solidification modeling", *Modeling Simul. Mater. Sci. Eng.*, Vol. 5, pp. 473-80.

Li, B.Q. (1994), "The fluid flow aspects of electromagnetic levitation processes", *International Journal of Engineering Science*, Vol. 32 No. 1, pp. 45-67.

Li, B.Q. and Anyalebechi, P.N. (1995), "A micro/macro model for fluid flow evolution and microstructure formation in solidification processes", *International Journal of Heat Mass Transfer*, Vol. 38, pp. 2367-81.

Marr, H.S. (1979), "Electromagnetic stirring: stepping stone to improved continuously cast products", *Iron & Steel International*, Vol. 2, pp. 29-41.

Rappaz, M. (1989), "Modeling of microstructure formation in solidification processes", *International Materials Reviews*, Vol. 34, p. 93.

Rappaz, M. and Gandin, Ch-A. (1993), "Probabilistic modelling of microstructure formation in solidification processes", *Acta metallurgica et materialia*, Vol. 41, pp. 345-60.

Shu, Y., Li, B.Q. and Ramaprian, B.R. (2005), "Experimental and numerical study of natural convection in oscillating thermal and gravity fields", *International Journal of Heat Mass Transfer*, Vol. 48, pp. 145-60.

Song, S.P. (1999), "Finite element analysis of surface oscillation, fluid flow and heat transfer in magnetically and electrostatically levitated droplets", PhD thesis, Washington State University, Pullman, WA.

Song, S.P. and Li, B.Q. (2000), "Electrically induced deformation and Marangoni convection in melt droplets under microgravity", *International Journal of Transport Phenomena*, Vol. 2, pp. 159-71.

Stefanescu, D.M. (2002), *Science and Engineering of Casting Solidification*, Kluwer Academic Publishers, New York, NY.

Stoehr, R.A. and Loyprasert, C. (1999), "Grain structure evolution in Al-Cu alloys solidifying during unidirectional flow over a chill: comparison of CA model with experiments", in El-Kaddah, N. *et al.* (Eds), *Fluid Flow Phenomenon in Metals Processing*, TMS, Warrendale, PA, pp. 441-8.

Vives, C. (1990), "Hydrodynamic, thermal and crystallographic effects of an electromagnetically driven rotating flow in solidifying aluminum alloy melts", *International Journal of Heat Mass Transfer*, Vol. 33 No. 12, pp. 2585-98.

Voller, V.R. and Brent, A.D. (1989), "The modeling of heat, mass and solute transport in solidification systems", *International Journal of Heat Mass Transfer*, Vol. 32 No. 9, pp. 1719-31.

Corresponding author
Ben Q. Li can be contacted at: benqli@umich.edu